Gravitational waves through the cosmic web

Garoffolo, A.

Part I

Ray-optics limit: beyond the homogeneous and isotropic Universe

2

Detecting the clustering of Dark Energy

Luminosity distance estimates from electromagnetic and gravitational wave sources are generally different in models of gravity where dark energy is a dynamical field beyond the standard cosmological scenario. This leaves a unique imprint on the angular power-spectrum of fluctuations of the luminosity distance of gravitational-wave observations, which tracks inhomogeneities in the dark energy field. Exploiting the synergy between supernovae and gravitational wave distance measurements, in this Chapter we build a joint estimator that directly probes dark energy fluctuations, providing a conclusive evidence for their existence in case of detection. Moreover, such measurement would also allow probing the running of the Planck mass. We discuss experimental requirements to detect these signals.

Keywords: Gravitational waves, DE clustering, luminosity distance fluctuations, number of sources

Based on: *Detecting Dark Energy Fluctuations with Gravitational Waves*

A. Garoffolo, M. Raveri, A. Silvestri, G. Tasinato, C. Carbone, D. Bertacca, S. Matarrese,

Phys.Rev.D 103 (2021) 8, 083506, e-Print: 2007.13722 [astro-ph.CO]

2.1. Introduction

Any theory attempting at providing a cosmological model must include predictions for the large-scale structures' dynamics. As a result, the dispositions of galaxies and the one of other tracers of the cosmic web, should contain footprints of any modification of the standard pictures. Scientific missions trying to characterize the spacetime always rely on the detection of a messenger: whether an electromagnetic (EMW) or a gravitational wave (GW). Therefore, the first detection of GWs has guaranteed a new observational window onto our Universe, promising to offer complementary probes to shed light on the dynamics of the Universe on cosmological scales. As described in Section 1.4.2, GW events at cosmological distances, in the geometric optics regime, can be used as *Standard Sirens* [197, 225, 234] for measuring the expansion rate of the Universe. This recent approach is complementary to measuring the luminosity distance of *Standard Candles*, like Type-Ia Supernovae (SNe): one of the two principal probes for the recent exponential expansion of the Universe [6, 7]. On the homogeneous and isotropic background, the luminosity distances depend only on redshift, leading to the standard distance-redshift relation tests as described in Section 1.4.2. After their emission, photons and gravitons travel through the dark matter gravitational potential wells, with the effect of spoiling the FLRW results regarding their luminosity distances to the sources. Inhomogeneities in the Universe induce a dependence of the distances also on the direction of observation in addition to redshift, $\Delta d_L(z, \hat{n})$, as described in Section 1.4.3. This additional dependence must be kept into account to perform accurate tests: distance measurements are reaching an unprecedented the level of precision, such that neglecting relativistic effects can bias our cosmological parameter inference. However, fluctuations in the luminosity distance do not only constitute a source of error: they give us direct access to the LSS. The possibility of having multi-messenger observations opened the powerful possibility of testing theoretical proposals which break the degeneracy between the GW and the electromagnetic sector. This is exactly the case for scalar-tensor theories of gravity described in Section 1.2, where photons, contrary to GWs, are not coupled directly to the DE scalar field. In presence of a dynamical DE field, the GW luminosity distance generally differs from the one traced by electromagnetic signals, both at the unperturbed, background level [183–190] and in its large-scale fluctuations [158, 235]. Importantly, fluctuations in the electromagnetic luminosity distance, $\Delta d_L^{\rm EM}$, are affected by the DE field only indirectly, as it can be seen in Eq (1.114), while the GW one, $\Delta d_L^{\rm GW}$, contains contributions directly proportional to the running Planck's mass, M_P and the clustering of the DE field, $\delta\varphi$, as it can be seen in Eq. (1.112). In this Chapter, we combine two standard distance indicators, SNe and GWs, and combine their luminosity distance fluctuations into a novel estimator to *directly* detect the signal of DE clustering. This signal can not be mimicked by other effects and would provide convincing evidence for the existence of the DE field. If DE does not directly couple to known particles through non-gravitational

interactions, the one proposed here is a promising method to pursue its direct detection, on cosmological scales, far from sources that can hide its presence by means of screening mechanisms (see e.g. [51, 236, 237]).

2.2. The GW luminosity distance power-spectrum

The luminosity distance, as inferred by an EM or GW signal propagating through a Universe with structures, depends on the observed redshift, z, and on the direction of arrival in the sky, $\hat{\theta}$. We decompose the observed luminosity distance of a source as a sum of its background and fluctuation components, as in Eq. (1.111). We use Eq. (1.112) to build the angular power-spectrum of GW luminosity distance fluctuations averaged over a given redshift distribution of the sources

$$C_\ell^{\rm GW} = 4\pi \int {\rm d}\ln k \left(\frac{\Delta d_L^{\rm GW}}{\bar{d}_L^{\rm GW}}\right)^W_{k\ell} \left(\frac{\Delta d_L^{\rm GW}}{\bar{d}_L^{\rm GW}}\right)^W_{k\ell}, \tag{2.1}$$

where we work in Fourier space for the perturbations, k being the momentum, and

$$\left(\frac{\Delta d_L^{\rm GW}}{\bar{d}_L^{\rm GW}}\right)^W_{k\ell} = \int_0^\infty dz\, j_\ell(k\chi)\, W(z) \left(\frac{\Delta d_L^{\rm GW}}{\bar{d}_L^{\rm GW}}\right), \tag{2.2}$$

and $j_\ell(x)$ is the spherical Bessel function and $W(z)$ is the source window function, normalized to 1. The effect of each term in Eq. (1.112) on the angular power-spectrum can be studied independently in terms of the different sources, highlighting each relativistic or modified gravity effect,

$$\left(\frac{\Delta d_L^{\rm GW}}{\bar{d}_L^{\rm GW}}\right)^W_{k\ell} = \int_0^{\tau_A} {\rm d}\tau\, j_\ell(k\chi) \Big\{ S_\kappa^{\rm GW} + S_{vol}^{\rm GW} + S_{Sh}^{\rm GW} + S_{SW}^{\rm GW} + S_{Dop}^{\rm GW} + S_{ISW}^{\rm GW} + S_{\delta\varphi}^{\rm GW} \Big\}, \tag{2.3}$$

with τ_A is the conformal time corresponding to $z = +\infty$ and

$$S_\kappa^{\rm GW}(\tau) = (\Phi_k + \Psi_k) \int_0^\tau {\rm d}\tilde{\tau}\, \frac{\ell(\ell+1)}{2}\, \frac{(\tilde{\chi}-\chi)}{\tilde{\chi}\chi}\, W(\tilde{\tau}) \tag{2.4}$$

$$S_{vol}^{\rm GW}(\tau) = -W(\tau)(\Phi_k + \Psi_k), \tag{2.5}$$

$$S_{Sh}^{\rm GW}(\tau) = (\Phi_k + \Psi_k) \int_0^\tau {\rm d}\tilde{\tau}\, \frac{W(\tilde{\tau})}{\tilde{\chi}} \tag{2.6}$$

$$S_{SW}^{\rm GW}(\tau) = W(\tau)\Big(\frac{1}{\chi\mathcal{H}} - \frac{M_P'}{\mathcal{H}M_P}\Big)\Psi_k, \tag{2.7}$$

$$S_{Dop}^{\rm GW}(\tau) = -\partial_\tau \left[W(\tau)\Big(1 - \frac{1}{\mathcal{H}\chi} + \frac{M_P'}{\mathcal{H}M_P}\Big) v \right] \tag{2.8}$$

$$S_{ISW}^{\rm GW}(\tau) = (\Phi_k' + \Psi_k') \int_0^\tau {\rm d}\tilde{\tau}\, W(\tilde{\tau}) \left(1 + \frac{M_P'}{\mathcal{H}M_P} - \frac{1}{\chi\mathcal{H}}\right), \tag{2.9}$$

$$S_{\delta\varphi}^{\rm GW}(\tau) = W(\tau)\, \frac{M_{P,\varphi}}{M_P}\, \delta\varphi \tag{2.10}$$

where $W(\tau) = (1+z)\,\mathcal{H}\,W(z)$. In (2.4) we assumed $v^i(k,\tau) = ik^i\,v(\tau)$, namely that the peculiar velocity field is irrotational. The reason why we introduced this notation is that it is more suitable for direct implementation of the calculation of $C_\ell^{\rm GW}$ in `EFTCAMB` [90]: the Einstein-Boltzmann solver code, described in Section 1.2.2, allowing us to study this quantity for a broad host of DE models. Note also that `EFTCAMB` evolves the perturbed gravitational field equations in terms of the rescaled DE field $\pi(x) = \frac{\delta\varphi(x)}{\varphi_0'(\tau)}$, assuming that $\varphi_0'(\tau) \neq 0$, as it is in a cosmological setting. Therefore, the last source among the ones above can be rewritten as

$$S^{\rm GW}_{\delta\varphi}(\tau) = W(\tau)\,\frac{M_{P,\varphi}}{M_P}\,\varphi_0'(\tau)\,\pi(x) = W(\tau)\,\frac{M_P'}{M_P}\,\pi(x)\,. \tag{2.11}$$

In order to explore in detail the impact of the DE field on $C_\ell^{\rm GW}$ we focus for a

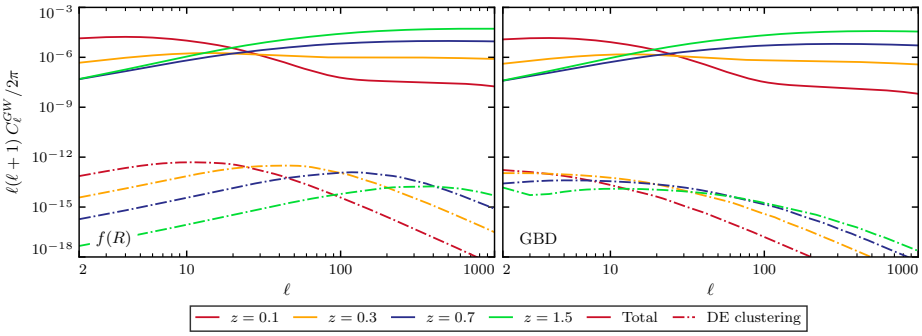

Figure 2.1: Angular power-spectrum of gravitational-wave luminosity distance fluctuations. Solid lines show the total power-spectrum, dashed lines the scalar field clustering component.

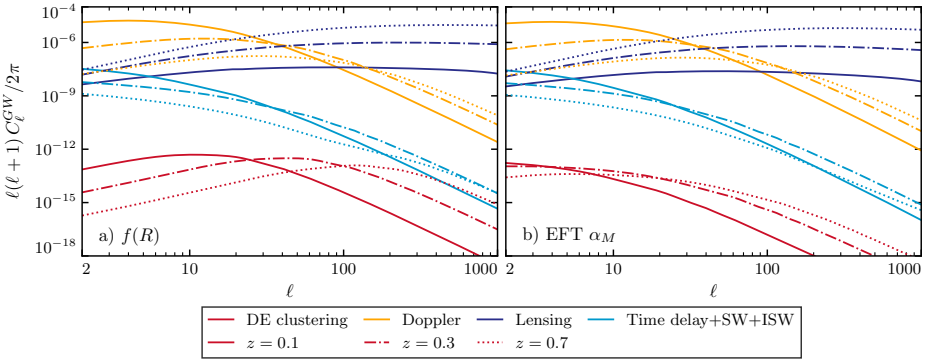

Figure 2.2: Various contributions to the angular power-spectrum of gravitational-wave luminosity distance fluctuations according to Eqs. (2.4)-(2.10). Solid, dashed and dotted contributions stand for increasing redshifts bins.

moment on two representative models. First, a designer $f(R)$ model on a ΛCDM

background [238], with the only model parameter set to $B_0 = 10^{-4}$ which is compatible with current constraints [239]. Second, an agnostic parametrization of M_P, such that the ratio (M_P'/M_P) is a linear function of the scale-factor, $a(z)$, $M_P'/M_P \equiv (M_P'/M_P)|_o\, a$, where $(M_P'/M_P)|_o$ is the value of the ratio today, which we set to 0.05. This minimal parametrization, implemented on a ΛCDM background, is representative of the Generalized Brans-Dicke (GBD) [240–242] family of theories. In both these models, the Planck mass M_P depends on the scalar field value alone, $\varphi_0(\tau)$.

Figures 2.1 and 2.2 show the angular power-spectrum, $C_\ell^{\rm GW}$, for the two scenarios described above. To highlight redshift dependencies, we choose a Gaussian distribution for the GW sources centered in various redshifts z_i, with width $\Delta z = 0.01$, i.e. $W(z) = \mathcal{N} \exp[-(z-z_i)^2/(2\Delta z^2)]$ where $\mathcal{N}$ is the normalization constant. The total signal significantly changes shape with increasing redshift. At low redshifts and large scales, the signal is dominated by the Doppler effect, encoded in $S^{\rm GW}_{Dop}(\tau)$, due to the bulk-flow of the environment in which the GW sources are embedded. The Doppler contribution then decays for growing ℓ, and the angular power-spectrum at small scales is dominated by lensing convergence, described in $S^{\rm GW}_\kappa(\tau)$; the Doppler term also decays in redshift, while lensing grows and eventually dominates the high-redshift part of the signal. This is a standard behavior: as lensing is an integrated effect, it accumulates throughout the propagation. These behaviors can be observed in Figure 2.2. For both models considered, the relative behavior between Doppler and lensing convergence is qualitatively unaltered with respect to the General Relativistic results [157]. Figure 2.1 also shows the direct contribution of $\delta\varphi$ to the total signal, i.e. $S^{\rm GW}_{\delta\varphi}$ of Eq. (2.10). This is of the same order of magnitude in both scenarios, and results largely subdominant compared to the total signal. For the $f(R)$ model, the scalar field contribution has a noticeable scale-dependent feature that evolves in time as the Compton wavelength of the model. At higher redshift, the Compton scale of the scalar field is smaller and, correspondingly, the feature in the power-spectrum moves to smaller scales. In the GBD case, on the other hand, any feature in the shape of the power-spectrum is less pronounced, as it only leads to the decay of DE fluctuations below the horizon.

2.3. The joint SNe/GW estimator

The direct contributions of DE fluctuations to $C_\ell^{\rm GW}$ are very small compared to other effects, making it impossible to detect their presence in the angular correlations using GW data only. Interestingly, since photons are not affected directly by DE or MG, $\Delta d_L^{\rm EM}$ is structurally unchanged w.r.t. the results of General Relativity, hence is obtained by neglecting all the explicit DE terms present in Eq. (1.112). The EM luminosity distance fluctuations, then, formally follow Eq. (1.114), with the gravitational potentials following the modified laws as described in Sections 1.2.2. We can single

out the distinctive DE field contributions, by combining standard sirens and standard candles: assuming that we have measurements of both SN and GW at the same redshifts and positions and subtract the two luminosity distances fluctuations as

$$\Delta_\varphi(\hat{n},z) \equiv \frac{\Delta d_L^{\rm EM}(\hat{n},z)}{\bar{d}_L^{\rm EM}} - \frac{\Delta d_L^{\rm GW}(\hat{n},z)}{\bar{d}_L^{\rm GW}}\,, \tag{2.12}$$

where the average luminosity distances are given in Eqs. (1.106) and (1.105). In what follows, we will use the estimator above in a statistical fashion. For this, we will need populations of GW and SN in overlapping regions of the sky and redshift bin, instead of having both events exactly in the same position and at the same redshift. For the theories considered here, Eq. (2.12) takes the form

$$\Delta_\varphi(\hat{\theta},z) = \frac{M_P'}{\mathcal{H}M_P}\left(\Phi - v_\parallel + \int_0^\chi d\tilde{\chi}\,(\Phi'+\Psi')\right) - \frac{M_{P,\varphi}}{M_P}\delta\varphi\,, \tag{2.13}$$

where only the explicit DE-dependent effects are present. In addition to the DE clustering contribution, only three effects contribute to Δ_φ: a residual Doppler, SW and ISW effects. Most importantly, lensing convergence, which is the dominant contribution to luminosity distance anisotropies, cancels out. Similarly as before, for the joint estimator Δ_φ we find the set of sources

$$\begin{aligned}
S_{SW}^{\Delta_\varphi}(\tau) &= W(\tau)\frac{M_P'}{\mathcal{H}M_P}\Psi \\
S_{Dop}^{\Delta_\varphi}(\tau) &= \partial_\tau\left[W(\tau)\frac{M_P'}{\mathcal{H}M_P}v\right] \\
S_{ISW}^{\Delta_\varphi}(\tau) &= -\left(\Phi_k'+\Psi_k'\right)\int_0^\tau \mathrm{d}\tilde{\tau}\,W(\tilde{\tau})\left(\frac{M_P'}{\mathcal{H}M_P}\right), \\
S_{\delta\varphi}^{\Delta_\varphi}(\tau) &= -W(\tau)\frac{M_{P,\varphi}}{M_P}\delta\varphi
\end{aligned} \tag{2.14}$$

For particular classes of events, Eq. (2.12) could be directly evaluated for pairs of sources at the same position and redshift. In our analysis we require this to hold only statistically, by integrating Eq. (2.12) over a joint redshift distribution and computing its angular power-spectrum:

$$C_\ell^{\Delta_\varphi} = C_\ell^{\rm SN} + C_\ell^{\rm GW} - 2C_\ell^{\rm SN-GW}\,, \tag{2.15}$$

where $C_\ell^{\rm SN}$ ($C_\ell^{\rm GW}$) are the SN (GW) luminosity distance angular power-spectra, and $C_\ell^{\rm SN-GW}$ the cross-spectrum between the two. In this form we need the redshift and position of GW/SNe sources to be the same only on average, i.e. same redshift distributions and overlapping regions in the sky. In Fig. 2.3 we show $C_\ell^{\Delta_\varphi}$ as a function of the source redshift for the two representative DE models. We consider the case of localized SN/GWs sources to study the redshift dependence of $C_\ell^{\Delta_\varphi}$. In $f(R)$, the DE clustering component is dominating the total angular power-spectrum, making its

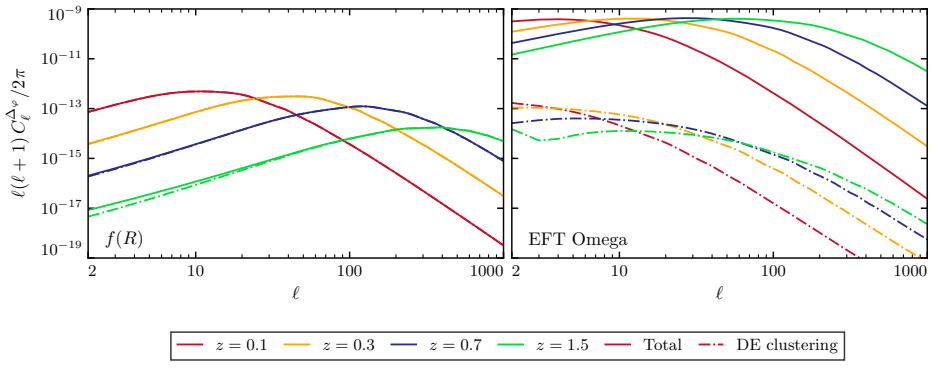

Figure 2.3: The angular power-spectrum of the difference between GW and SN luminosity distance fluctuations. Solid lines show the total power-spectrum, dashed lines the scalar field clustering component.

features manifest. In the GBD model, instead, the total signal is dominated by the Doppler effect. Nevertheless, a detection of this signal still constitutes a direct proof of the DE field's presence.

2.4. Observational prospects

We next investigate the detection prospects for the fluctuations of the GW luminosity distance via $C_\ell^{\rm GW}$, and DE clustering via $C_\ell^{\Delta_\varphi}$. We consider the noise power-spectrum for both SN and GW, as given by only a shot-noise contribution [243, 244]:

$$N_\ell^i = \frac{4\pi f_{\rm sky}}{N_i}\left(\frac{\sigma^i_{d_L}}{d^i_L}\right)^2 \equiv \frac{4\pi f_{\rm sky}}{N_i^{\rm eff}}\,, \tag{2.16}$$

where $i = \{\rm SN, GW\}$ and $f_{\rm sky}$ is the sky fraction covered by observations, which we assume to be $f_{\rm sky} = 1$ for simplicity. We also define the effective number of sources, $N_i^{\rm eff}$, as the product of the number of events, N_i, in a given redshift bin and the ratio $\sigma^i_{d_L}/d^i_L$ related to the relative uncertainty on the luminosity distance which is proportional to the magnitude uncertainty. In this way $N_i^{\rm eff}$, which sets the overall noise levels, takes into account the number of events detected and the precision of each measurement. As the signal decays in scale faster than $\propto \ell^{-2}$, we expect to have the best chance of measuring it from large-scale observations. For this reason we assume that future localization uncertainties can be neglected [245].

The noise for the joint estimator of Eq. (2.15) is given by the sum of the two noise power-spectra for GW and SN, since we assume that any stochastic contribution is uncorrelated. Consequently, the number of effective events needed for a detection

of $C_\ell^{\Delta_\varphi}$ is given by the harmonic mean of the two single ones

$$N_{\Delta_\varphi}^{\rm eff} = \left[\frac{1}{N_{\rm SN}^{\rm eff}} + \frac{1}{N_{\rm GW}^{\rm eff}} \right]^{-1} . \tag{2.17}$$

2

The error on a power-spectrum measurement is given by

$$\sigma(C_\ell) = \sqrt{2/(2\ell+1) f_{\rm sky}}\, [\, C_\ell + N_\ell \,] \,, \tag{2.18}$$

and the corresponding signal-to-noise ratio is

$$\frac{S}{N} = \sqrt{\sum_\ell \left(\frac{C_\ell}{\sigma(C_\ell)} \right)^2} . \tag{2.19}$$

In the case of $C_\ell^{\rm GW}$ this applies directly, while for $C_\ell^{\Delta\varphi}$ one needs to do full error propagation on Eq. (2.15): the final result is the same, provided one uses for $N_{\Delta_\varphi}^{\rm eff}$ the harmonic mean given above. The noise power-spectrum in Eq. (2.16) is scale-independent so we can solve the inverse problem of determining the number of effective events needed to measure the power-spectra with a desired statistical significance. In practice, we fix a target $S/N = 5$, and solve the equation of S/N for $N^{\rm eff}$ both in the case of GW sources alone and Δ_φ. Finally, we investigate the scenario where the GW source redshift is unknown. In this case we assume the shape of the GW redshift distribution as given in [220], while the SN one as in [246]. Since the SN and GW redshift distributions need to match for our estimator to work, we take the product of the two and build the joint probability of measuring both SN and GW at the same redshift. In particular, we consider

$$\frac{dN^{\rm GW}(z)}{dz} = \mathcal{N}_{\rm GW} \frac{\chi^2(z)}{(1+z)^2 \mathcal{H}} , \qquad \frac{dN^{\rm SN}(z)}{dz} = \mathcal{N}_{\rm SN} \times \begin{cases} 2.5 \, \dfrac{\chi^3(z)}{(1+z)^{1.5}} & z < 1 \\ 9.7 \, \dfrac{\chi^3(z)}{(1+z)^{3.5}} & z \geq 1 \end{cases} , \tag{2.20}$$

where $\mathcal{N}_{\rm GW}$ and $\mathcal{N}_{\rm SN}$ are suitable normalization. Even if such redshift distributions depend on the cosmological model (for instance through $\mathcal{H}(z)$), we use their ΛCDM expressions, as we have checked that this dependency is negligible. Intermediate cases in which the EM counterpart is not available, but estimates of the redshift distributions are obtained via statistical methods [207, 209, 247, 248], would fall in between the two extreme cases examined here.

Table 2.1 summarizes the results reporting the number of effective sources for a 5σ detection of the angular power-spectra $C_\ell^{\rm GW}$ and $C_\ell^{\Delta_\varphi}$, both in the case of GW events with known as well as unknown redshifts (the latter designated as "w/o z"). We also indicate the value of $N_{\rm GW}^{\rm eff}$ in General Relativity, for comparison. The detection threshold for GW luminosity distance fluctuations, $N_{\rm GW}^{\rm eff}$, does not change appreciably for the different scenarios, since we selected representative models sufficiently

	GR	$f(R)$		GBD	
	$N^{\rm eff}_{\rm GW}$	$N^{\rm eff}_{\rm GW}$	$N^{\rm eff}_{\Delta_\varphi}$	$N^{\rm eff}_{\rm GW}$	$N^{\rm eff}_{\Delta_\varphi}$
$z=0.1$	10^7	10^7	10^{14}	10^7	10^{12}
$z=0.3$	10^8	10^8	10^{15}	10^8	10^{11}
$z=0.7$	10^8	10^8	10^{16}	10^8	10^{12}
$z=1.5$	10^7	10^7	10^{17}	10^7	10^{12}
w/o z	10^7	10^7	10^{19}	10^7	10^{14}

Table 2.1: Effective number of events for a 5-σ detection of $C_\ell^{\rm GW}$ and $C_\ell^{\Delta_\varphi}$.

close to ΛCDM to satisfy current constraints. In fact, as shown in Fig. 2.1, $C_\ell^{\rm GW}$ is dominated by lensing convergence at high redshifts and by Doppler shift at low redshifts. The former is *indirectly* modified by DE, while the latter is also sensitive to the background configuration of the DE field: both these effects are small in the considered models. Since lensing convergence and Doppler effect dominate the angular correlations of GW sources, it is not possible to distinguish the DE clustering contribution in $C_\ell^{\rm GW}$ within the total signal.

As far as $N^{\rm eff}_{\Delta_\varphi}$ is concerned, the results show that it is possible to detect the signal of the joint estimator in both cases of known and unknown redshifts. In $f(R)$, this signal is dominated by the DE field fluctuations, as shown in Fig. 2.3, hence allowing for its direct detection. In the GBD model, the signal of the joint estimator is dominated by Doppler shift, easier to detect, explaining the lower number of effective events compared to $f(R)$. In this case, one would not be able to distinguish directly the DE field inhomogeneities, but its detection is still a proof of a time-dependent Planck mass. Comparing the two scenarios of known and unknown GW source's redshift, we see that the number of effective events is larger in the latter case because a broader redshift range weakens the signal. However, in this situation the events are not restricted to a redshift bin, hence one can use the whole population of SN/GW sources provided that they are both present. Nonetheless, the number of effective events required is very high, suggesting that the detection precision per source has to improve to eventually measure such signal. In fact, we remark that $N_i^{\rm eff}$ is the effective number of sources, *the real number of events can be lowered by having smaller statistical errors on the single detection.* As an example, in order to measure the DE signal, the detection of a population of about 10^6 GW sources and about the same number of SN events in a redshift bin at $z>1$, would require a precision, per event, of about $\sigma_{d_L}/d_L \sim 10^{-6}$ in the case of $f(R)$, and $\sim 10^{-3}$ for the GBD model. Since the required effective number of events scales quadratically with per-event precision, σ_{d_L}/d_L, but

only linearly with number of events, increasing precision is likely a better strategy.

2.5. Discussion and Conclusions

Fluctuations in the DE field can distinctively alter the propagation of GWs with respect to light. In this Chapter, by combining the luminosity distance measurements from GW and SN sources, we proposed the new estimator Δ_φ for the *direct* detection of the imprint of the DE fluctuations, that does not rely on non-gravitational interactions between DE and known particles. This signal cannot be mimicked by other effects and, as such, it provides a distinctive evidence for a dynamical DE model. Even in the case of a DE clustering signal below cosmic variance, any detection of our joint estimator would be a convincing proof of a running Planck mass, as we showed for two specific models. Reversely, it can be used to place complementary bounds on theories of dynamical dark energy non-minimally coupled to gravity, along similar lines of recent forecasts as in [161, 249] for the case of standard sirens. Since we exploit angular correlations at large scales, we expect our method not to be affected by screening mechanisms nearby sources.

Since the required effective number of source is quite large, one should leverage as much as possible on the precision of the measurement; for instance, given the number of SN/GW events (of order 10^6, at least in the higher redshift bins) that can be observed with future SN surveys [12, 250] and space-based interferometers [251, 252], a detection would be possible, if one decreases the statistical error on each measure according to table 2.1. Notice also that for our estimates we considered an ideal case: the number of events needed for a detection might be higher to deal with possible systematic effects. This suggests that future facilities might have to develop new technologies and observational strategies to meet these detection goals. We leave it to future work to determine whether a detection of the signal we propose can be aided by studying additional DE models, synergies with large scale structure surveys or considering different sources of GW/EM signals. For example, future experiments will detect large numbers of binary white dwarfs [253] on galactic scales and much beyond [254, 255]. These events are supposed to be progenitors of Type-Ia SN in the so-called double degenerate scenario [256], offering a common source for GW and SN signals (see e.g. [257]). In this case, Eq. (2.12) holds locally and Δ_φ could be directly reconstructed in configuration space, provided that non-linearities and DE screening effects can be properly taken into account.

Note: My contribution to the paper this Chapter is based on regards all the scientific aspects, both theoretical and numerical, and the writing.